Journal of Alloys and Compounds 509 (2011) 2723–2728

Contents lists available at ScienceDirect

Journal of Alloys and Compounds

journal homepage: www.elsevier.com/locate/jallcom

Thermal expansion and lattice parameters of shaped metal deposited Ti–6Al–4V

Akhilesh Kumar Swarnakar, Omer Van der Biest, Bernd Baufeld*

Katholieke Universiteit Leuven, MTM, Kasteelpark Arenberg 44, 3001 Leuven, Belgium

ARTICLE INFO

Article history:
Received 2 November 2010
Received in revised form
30 November 2010
Accepted 1 December 2010
Available online 9 December 2010

Keywords:
Shaped metal deposition
Titanium alloy
Thermal expansion
High temperature X-ray diffraction
Phase transformation

ABSTRACT

Thermal expansion and lattice parameters are investigated up to 1100 °C for Ti–6Al–4V components, fabricated by shaped metal deposition. This is a novel additive layer manufacturing technique where near net-shape components are built by tungsten inert gas welding.

The as-fabricated SMD Ti–6Al–4V components exhibit a constant coefficient of thermal expansion of $1.17 \times 10^{-5}\ K^{-1}$ during heating up to 1100 °C, not reflecting the α to β phase transformation. During cooling a stalling of the contraction is observed starting at the β transus temperature. These high temperature experiments denude the α phase of V and enrich the β phase.

The development of the lattice parameters in dependence on temperature are observed with high temperature X-ray diffraction. The unit cell volumes derived from these parameters are at room temperature larger for the α than for the β phase. With increasing temperature the unit cell volume of the β phase increases stronger than the one of the α phase resulting in a similar unit cell volume at the β transus temperature.

These observations are interpreted as an indication for as-fabricated the SMD components being in a non-equilibrium state and reaching equilibrium during the slow heating and cooling during of the two different high temperature experiments.

1. Introduction

Titanium alloys are widely used when excellent strength to weight ratio [1], superior biocompatibility, low elastic modulus and/or enhanced corrosion resistance are needed [2]. Examples for this can be found, for example, in applications for aerospace, implants, and sports equipment [1–3]. One of the most widely applied Ti alloy is Ti–6Al–4V [3].

Ti is a costly metal and traditional machining of Ti alloys is expensive and time consuming. It is especially difficult to machine since it is prone to oxygen contamination at high temperatures. This contamination results into the formation of a brittle surface layer, the so-called α case [4,5]. In order to avoid this α case, low machining rates are required which increases the machining time and the costs.

Hence, near net-shape production by innovative manufacture routes would be of great advantage, which in addition would reduce the amount of scrap and the fabrication time to the end product. So-called additive layer manufacturing can fulfil these requirements. Several techniques are currently under investigation, where different heat sources such electron beam [6–9], laser [9–18], or a welding torch [19–29] are applied. The later is called shaped metal deposition (SMD), a technique patented by Rolls Royce, which is the topic of the present paper.

Additive layer manufacturing allows rapid fabrication of 3D objects, layer by layer directly from a computer aided design data source. Furthermore, it is promising in small-scale production of parts and for repair of high performance alloy components. However, additive layer manufacturing in general, and therefore also SMD, exhibits a rather peculiar fabrication scheme with repeated exposure to high temperatures, thermal gradients and cooling rates. This peculiar thermal history has a major impact, since the morphology and therefore the properties of Ti alloys depend critically on it. For example, the Ti–6Al–4V equilibrium phase diagram predicts at high temperatures the body centred cubic β phase and a α + β phase field below 1000 °C (Fig. 1). When, during manufacturing, these different phase fields are traversed, different morphologies can be obtained depending on the cooling rate [30–33]. Colony structures and basket weave Widmanstätten structures with α phase lamellae in a residual β phase matrix do occur during slow or medium fast cooling rates. At very high cooling rates (>410 °C/s) diffusion based transformation to the α + β phase may be omitted and passing the MS line (Fig. 1), the result is a fully martensitic hcp α′ phase microstructure [32]. Naturally, also intermediary or mixed states may arise. Not only the morphology, but also the composition of the phases may depend on the thermal history. For example, for higher cooling rates a departure from the

* Corresponding author. Present address: NAMRC, University of Sheffield, Brunel Way, Catcliffe, Rotherham S60 5WG, UK.
E-mail address: b.baufeld@sheffield.ac.uk (B. Baufeld).

0925-8388/$ – see front matter © 2010 Elsevier B.V. All rights reserved.
doi:10.1016/j.jallcom.2010.12.014

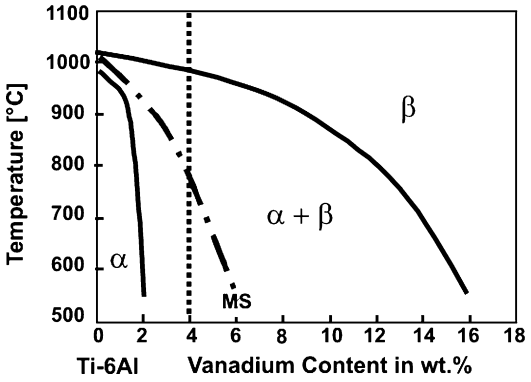

Fig. 1. Schematic ternary phase diagram Ti–6Al–V (MS: martensite start temperature) after [3]. Copyright Wiley-VCH Verlag GmbH & Co. KGaA. Reproduced with permission.

equilibrium phase boundaries can be expected, decreasing the size of the α + β phase field [34], and leading to an α phase composition higher in vanadium and poorer in aluminium than in the equilibrium case. The non-equilibrium β phase composition would then be lower in vanadium and higher in aluminium.

It has been shown elsewhere, that Ti–6Al–4V SMD components consist mainly of α lamellae in a β matrix, either colony or basket weave Widmanstätten, with no indication for the martensitic α′ phase [25,26]. Furthermore, it has been demonstrated, that this material is highly textured, and that the β to α transformation obeys the Burgers orientation relationship [25]. This microstructure differs significantly from the one in material fabricated by conventional techniques, and the properties can therefore not necessarily be simply deduced. The goal of the present paper is to investigate the thermal expansion and relate it with the lattice parameters measured by X-ray diffraction (XRD).

2. Experimental

2.1. Shaped metal deposition

The SMD cell consists of a tungsten inert gas (TIG) welding head, attached to a 6-axis Kuka robot linked to a 2-axis table, all of which are enclosed in an airtight chamber. The setup is located at the AMRC, Sheffield, United Kingdom. In the present case, a Ti–6Al–4V grade 5 wire with a diameter of 1.2 mm in an inert argon atmosphere (99.999% purity) is applied to build a component. Layer by layer, with rotating the table to keep a constant torch direction, a tubular shape with squared cross-section (0.15 m × 0.15 m), a height of 0.12 m, and a wall width of 0.01 m was built. The controlled parameters were the wire feed speed of 2.4 m/min, the table speed of 0.3 m/min and the electrical current of 150 A.

2.2. Thermal mechanical analysis

The thermal expansion in dependence on the temperature has been measured by the Netzsch DIL 402C dilatometer, a set-up also called TMA (thermo-mechanical analysis), in vacuum up to 1100 °C with a heating and cooling rate of 2 °C/min. Generally, before starting the TMA the vacuum chamber was flushed three times with argon and evacuated. In one case, the chamber was pumped after the third flushing for a whole day resulting in a better vacuum than in the case of starting the test after pumping for 1 h after the third flushing.

2.3. X-ray diffraction including high temperature measurements

The room temperature X-ray diffraction (XRD, 3003-TT, Seifert, Ahrensburg, Germany) was carried out in ambient atmosphere. The high temperature diffraction experiments (HT-XRD) were performed with the same diffractograph in continuous flow of Ar applying in addition a high temperature furnace (HDK 2.4 X-ray furnace, Johanna Otto, Hechingen, Germany). The testing temperatures were 50 °C and further from 300 up to 1100 °C increasing in 200 °C steps. The same temperatures were investigated during cooling down. The room temperature XRD was performed in the 2Θ range from 20° to 120° with a step size of 0.02° and a scan step time of 2 s. The HT-XRD was performed in the 2Θ range from 30° to 95° with a step size of 0.05° and a scan step time of 1 s.

As already mentioned, the Ti–6Al–4V SMD components are highly textured and in some sense can be considered as pseudo-single-crystalline [25]. The diffraction pattern of such highly textured component depends critically on the orientation of the component relative to the X-ray beam and frequently the required Bragg condition is not accomplished. Hence, the appearance and the height of diffraction peaks usually do not agree with the one derived from powders. A consequence of this is that the relative amount of two phases cannot be derived from the relative intensities. Yet, if a diffraction peak appears, the diffraction angle 2Θ can be used, applying Bragg's law, to determine the distance of the reflecting planes *d*. With the reflecting planes the lattice parameter can be derived. For hexagonal closed packaged structures, such as the α phase, the lattice parameters *a* and *c* can, for example, be calculated using the [1 0 0], [1 1 0], [0 0 2], and [1 0 2] reflections:

$$a = d_{100}\frac{2}{\sqrt{3}} \quad (1)$$

$$a = 2d_{110} \quad (2)$$

$$c = 2d_{002} \quad (3)$$

$$c = \frac{2}{\sqrt{(1/d_{102}^2) - (4/3)(1/d_{110}^2)}} \quad (4)$$

For bbc structures, such as the β phase, the lattice parameter *c* can be derived by:

$$c = 2d_{200} \quad (5)$$

The unit cell volume *V* then is

$$V_a = \frac{\sqrt{3}}{2}ca^2 \quad \text{or} \quad V_\beta = c^3 \quad (6)$$

The average length *L* for the unit cell, which will be taken as a measure for length changes, can be approximated by

$$L = \sqrt[3]{V} \quad (7)$$

2.4. Scanning electron microscopy including EDX

The microstructure was investigated by scanning electron microscopy (SEM, FEI XL30FEG) of polished cross-sections, where back-scattered electron (BSE) imaging with very high contrast allows discerning directly the α and β phases, omitting artefacts from etching. Energy dispersive X-ray (EDX) point analysis was applied to determine the composition of the phases.

2.5. Micro-Vickers hardness

The Vickers microhardness tests were performed on polished cross-sections of as-fabricated specimens and of specimens tested by IET or TMA applying a Leitz/Durimet 2 microhardness tester using a weight of 100 g (HV0.1).

3. Results

3.1. Thermal mechanical analysis

During heating in a good vacuum the SMD specimen exhibits continuous linear expansion until 1100 °C, not exhibiting any variation while passing the α + β phase field or reaching the β phase field (Fig. 2(a)). Hence, in the case of as-fabricated material, phase transformations are not reflected in the TMA. The coefficient of thermal expansion (CTE) during heating is $1.17 \times 10^{-5}\,K^{-1}$. During cooling, first the contraction line follows the expansion line until reaching the β transus temperature at 1000 °C. Then, the contraction stalls until about 900 °C. Further on, again linear contraction is observed with a slope similar to the expansion. The stalling during heating between 1000 and 800 °C results into a hysteresis and a net-increase of the specimen length of about 0.1%.

The experiment in the poorer vacuum shows the influence of oxygen (Fig. 2(b)). During heating, until about 800 °C a similar CTE as in the case of the good vacuum is observed. At higher temperatures, however, increased expansion is recorded. Also, during cooling, in the regime between 1100 and 1000 °C, the contraction rate is slightly lower than the observed expansion rate during heating. Therefore, due to the poorer vacuum the hysteresis is opened up more and a net-increase of the specimen length of about 0.2% is observed. However, the general result in both cases is the same: during heating the phase transformation from α to β is not reflected in the TMA curve, while during cooling the transformation from β to α phase results in an increased length.

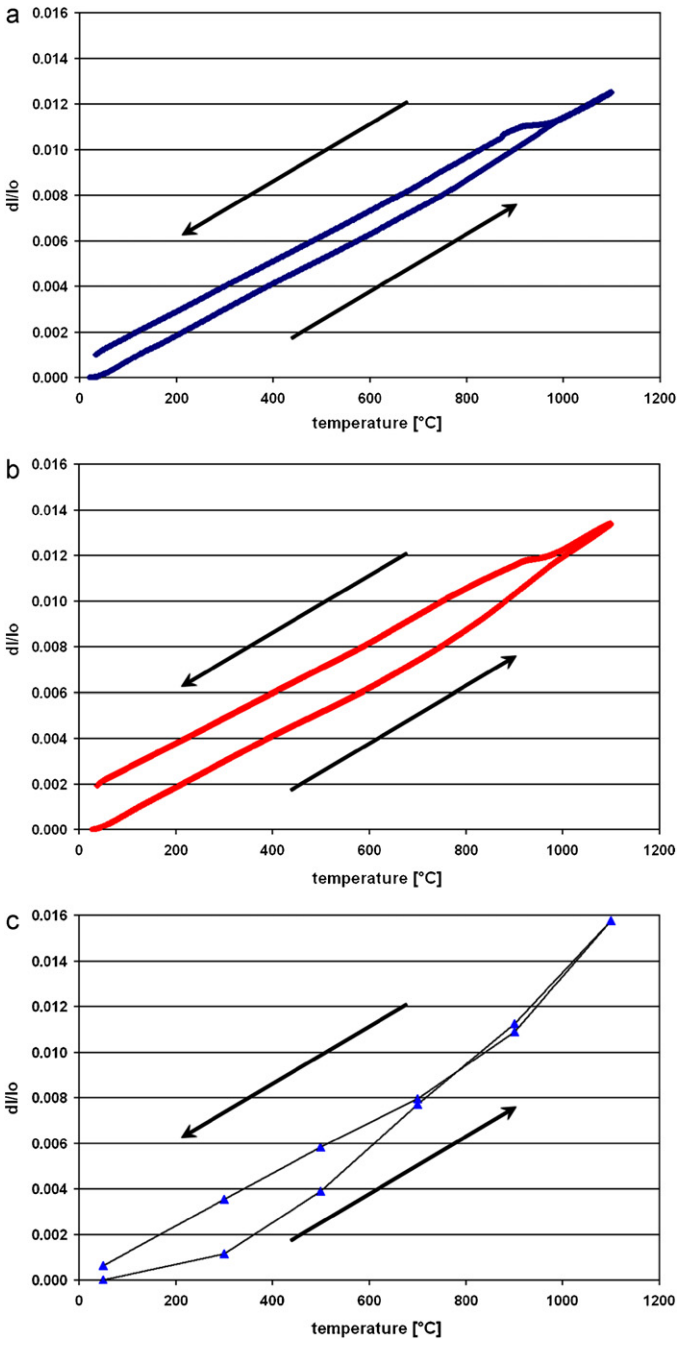

Fig. 2. TMA curves showing the relative length change in dependence on the temperature in the case of good (a) and poorer (b) vacuum. (c) Relative length change derived from the unit cell volume measured by the HT-XRD (derived from $[1\,1\,0]_{\alpha}$, $[1\,0\,2]_{\alpha}$, and $[2\,0\,0]_{\beta}$ reflections). The arrows indicate the heating (up) and the cooling (down).

After TMA up to 1100 °C the surfaces of the specimens are dull indicating oxidation at the surface. The specimen tested in the poorer vacuum even exhibits oxide flakes spalling off during handling after the test.

3.2. X-ray diffraction including high temperature measurements

Fig. 3 shows the diffraction patterns before and after TMA. All peaks can be attributed to Ti α phase. After TMA some peaks are weaker than before or are not appearing at all. This is attributed to slightly different orientations of the specimen in connection with the strong texture, as discussed before. No reflections belonging to

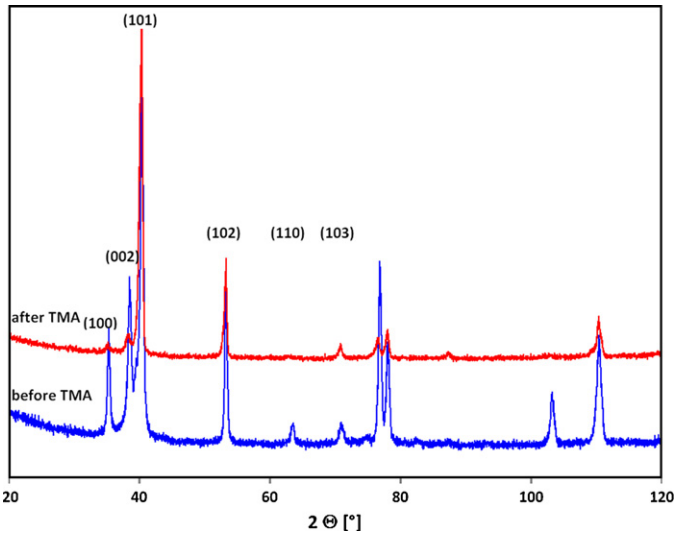

Fig. 3. X-ray diffraction pattern at room temperature before and after TMA.

the β phase appear which can be explained by the low amount of the β phase in combination with orientations not fulfilling Bragg's law for the β phase. The lattice parameters derived from the different reflections are given in Table 1. It appears, that both lattice parameters *a* and *c* of the α phase, and therefore also the unit cell volume *V*, have increased due to the TMA experiment. This increase gives, applying Eqs. (6) and (7) (only for the α phase, since no reflections of the β phase were detected), a net length increase of about 0.5%.

Fig. 4 exhibits the HT-XRD patterns, where all besides one peak belong to the α phase. The additional peak can be identified to be the [2 0 0] reflection of the β phase [35]. With increasing temperature the peaks shift to the left and the [2 0 0] reflection of the β phase increases in intensity. At 1100 °C the α phase reflections have disappeared and the [2 0 0] reflection of the β phase is the only remaining. It is noteworthy that this peak exhibits at 1100 °C a broad shoulder. Cooling down, the α phase reflections reappear, but not necessarily the one observed in the as-fabricated state. For example, during cooling down the [2 0 1] reflection now is very dominant, but the [1 0 0] does not exist anymore. With cool-

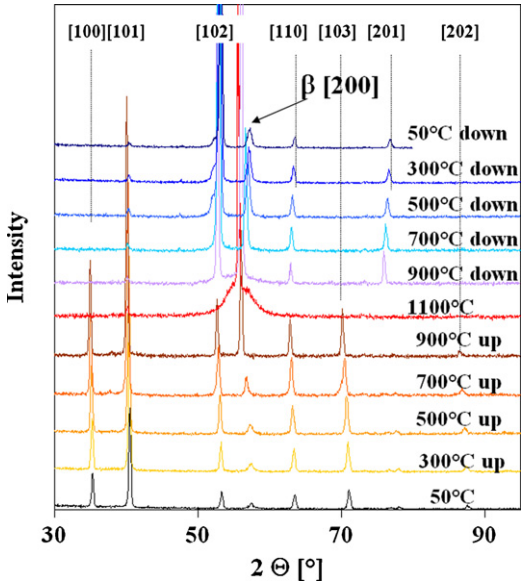

Fig. 4. High temperature diffraction patterns.

Table 1
Lattice parameters and unit cell volume at room temperature, derived from different XRD reflections (as indicated) before and after TMA, respectively HT-XRD.

		Before TMA	After TMA	Before HT-XRD	After HT-XRD
α phase	a_{100} [Å]	2.931	2.946	2.934	–
	a_{110} [Å]	2.928	–	2.928	2.926
	c_{002} [Å]	4.669	4.696	–	–
	$c_{102\,110}$ [Å]	4.676	–	4.669	4.679
	$V_{100\,002}$ [Å^3]	34.74	35.28	–	–
	$V_{102\,110}$ [Å^3]	34.73	–	34.66	34.68
β phase	c_{200} [Å]	–	–	3.203	3.216
	V_{200} [Å^3]	–	–	32.86	33.26

ing down, the intensity of the [2 0 0] reflection of the β phase has decreased significantly.

Fig. 5 shows the development of the unit cell volumes V of the α and the β phase during heating and cooling of the HT-XRD experiment. The unit cell volume of the α phase V_α changes fairly linear during heating and cooling and is only slightly larger after the HT-XRD experiment. The unit cell volume of the β phase V_β is at room temperature significantly smaller than the one of the α phase. However, during heating the unit cell volume V_β increases more pronounced and at the β transus temperature (1000 °C) both phases have supposedly the same unit cell volume. During cooling again a prominent change in the unit cell volume is observed. After the HT-XRD the unit cell volume of the β phase is larger than before.

The unit cell volumes and the lattice parameters at the beginning and at the end of the HT-XRD experiment are summarized in Table 1. Apparently the HT-XRD has increased V_α slightly, but V_β significantly. Assuming an amount of 10% of the β phase as typically observed for Ti–6Al–4V at room temperature, the change of V_α and V_β gives a net increase in length of 0.1%, which agrees with the TMA result in a good vacuum.

The lattice parameters derived from different reflections and different as-fabricated specimens agree well with each other, and give $a = 2.93$ Å and $c = 4.67$ Å for the α phase and $c = 3.20$ Å for the β phase. The relative average length of the unit cell volume, derived from $[1\,1\,0]_\alpha$, $[1\,0\,2]_\alpha$, and $[2\,0\,0]_\beta$ reflections, is plotted in Fig. 2(c) to compare with the TMA results (Fig. 2(a) and (b)). For simplicity, a β phase volume amount of 10% has been assumed for temperatures below 1000 °C and of 100% for 1100 °C. The dependence of the relative average length of the unit cell volume on temperature is quite similar to the one measured with TMA indicating that the assumptions made for the calculations are in the right order of magnitude. However, the details measured by TMA, specifically the stalling during cooling, could not be reproduced.

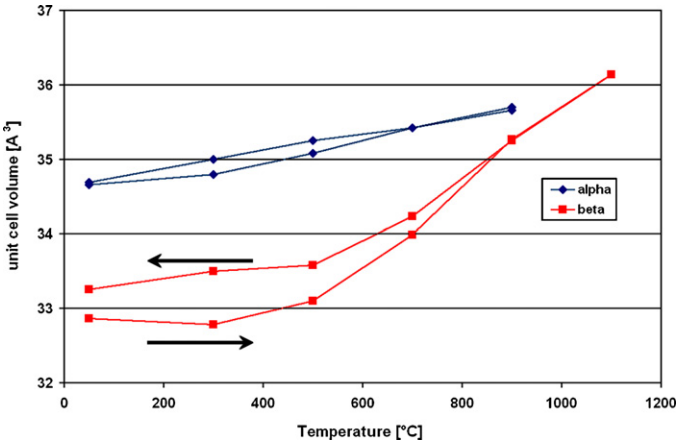

Fig. 5. Unit cell volumes of the α and the β phase in dependence on the temperature during HT-XRD (derived from $[1\,1\,0]_\alpha$, $[1\,0\,2]_\alpha$, and $[2\,0\,0]_\beta$ reflections). The arrows indicate the directions of the temperature change.

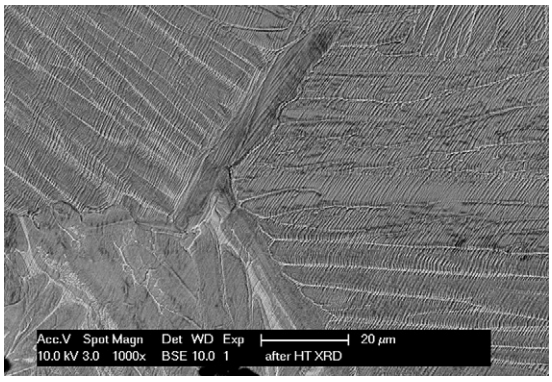

Fig. 6. Thermally etched surface after HT-XRD exhibiting lamellae and surface steps.

After the HT XRD experiment the specimen is still shiny indicating that in contrast to the TMA experiments no oxygen contamination took place. The former polished planes now exhibit a surface relief revealing grains and lamellae and surface steps (Fig. 6). This surface relief is interpreted as the result from thermal etching due to preferential evaporation at different rates on different crystallographic planes [36].

3.3. Scanning electron microscopy including EDX

The microstructure of as-fabricated Ti–6Al–4V SMD components (Fig. 7(a)) comprises of α phase lamellae (grey contrasts) in a β matrix (white contrast). These lamellae may form a basket weave Widmanstätten structure (Fig. 7(a)), or, especially near the component surfaces, colony structures. Always only bimodal α/β structures were found, which indicates diffusion and therefore excludes the diffusionless martensitic formation of the α′ phase. Apparently, the SMD process supplied not high enough cooling rates for the martensitic transformation and/or formed martensites were retransformed during subsequent SMD steps, which subjected already deposited material to temperatures above than the MS line [37]. More details about the microstructure can be found elsewhere [25,26].

After TMA, the lamellae are much coarser, but still exhibit Widmanstätten structure (Fig. 7(b)). In addition, near the surface a α case has been formed, where alloying of oxygen stabilizes the α phase, preventing residual β phase. The TMA has changed the composition of the phases (Table 2). Most significantly, the α phase

Table 2
Composition of the α and β phase before and after TMA, as determined by EDX.

		Ti [wt.%]	Al [wt.%]	V [wt.%]
α phase	As-fabricated	92.0 ± 0.5	5.7 ± 0.1	2.3 ± 0.6
	After TMA	91.7 ± 0.5	6.9 ± 0.5	1.4 ± 0.9
β phase	As-fabricated	89.6 ± 0.5	5.0 ± 0.4	5.4 ± 0.9
	After TMA	76.9 ± 3.2	3.5 ± 0.4	19.6 ± 2.9

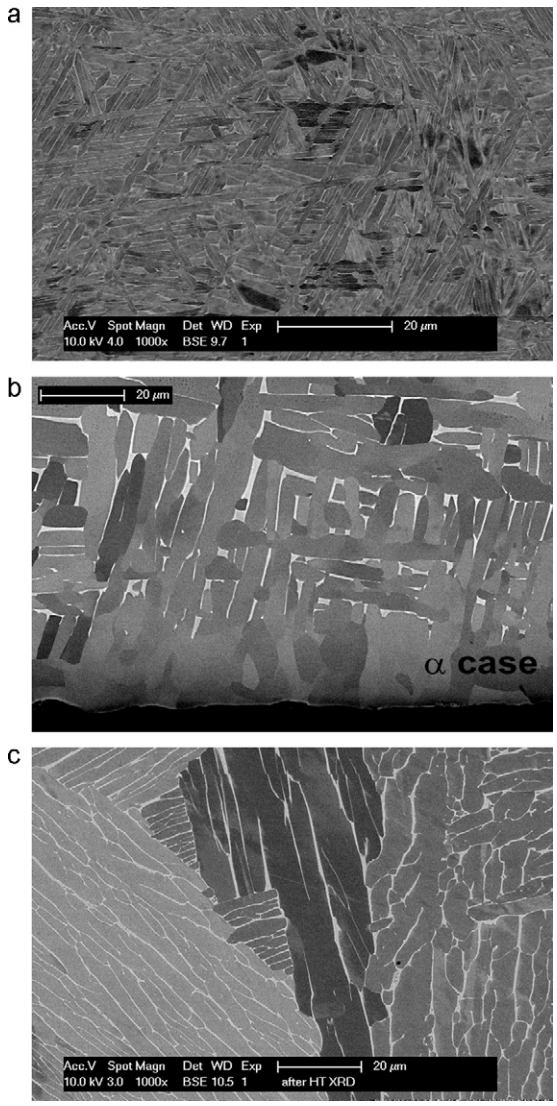

Fig. 7. Microstructures in the as-fabricated state (a), after TMA including the α case at the surface (b) and after HT-XRD (c).

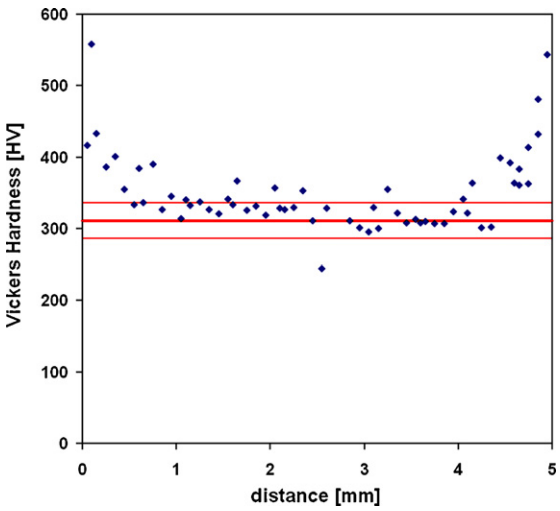

Fig. 8. Vickers microhardness of a cross-section of the specimen after TMA. The lines indicate the average value (bold line) of the as-fabricated SMD component including the variance (thin lines).

has a decreased amount in vanadium and an increased amount in aluminium, and the β phase has a largely increased amount in vanadium. Precise values for the β phase can, however, not be determined reliably, since their size is too small compared to the size of the electron beam and neighbour areas influence the result.

After the HT-XRD experiment, no Widmanstätten microstructure was observed but only large colonies of coarsened α lamellae in a β matrix (Fig. 7(c)), which is typical for slow cooling rates [30,32].

3.4. Vickers hardness

As fabricated the SMD component has a Vickers microhardness of 311 ± 25 HV0.1. After TMA, the μVickers hardness varies across the whole width of the specimen. Near the surfaces the values are largely increased up to almost 600 HV0.1 (Fig. 8). In the centre, the values are 322 ± 22 HV0.1, which are comparable or possibly slightly larger than for as fabricated components. In the case of HT XRD no change in hardness was observed.

4. Discussion

Astonishingly not much published work can be found about thermal expansion on α/β Ti, and all of these are not additive layer manufactured, but fabricated by conventional routes. Furthermore, the few reports concerning the thermal expansion of α/β Ti are rather contradicting. Carvalho et al. [38] report for Ti-6242 a dilatometry curve during heating similar to the cooling curve of the present work and a cooling curve similar to the heating curve of the present work. They claim that the α–β transformation cannot be responsible for the observed stalling of the expansion during heating and speculate that interstitials, particularly oxygen may be responsible. They argue that possibly during heating these interstitials may outgas in the high vacuum resulting in the stalling of the expansion.

Tarin et al. [39,40] report a totally different dilatometry curve for their Ti alloys. During heating their alloys expand first linearly until 900 °C, then the expansion increases drastically until about 950 °C, and from 950 until 1000 °C approximately the original expansion rate was obtained, which is also similar to the contraction rate during the whole cooling until room temperature. They attributed the drastic increase of the expansion to the α to β transformation but do not discuss why the β to α transformation during cooling does not appear in a similar way.

Robert reports in his thesis [41] other types of dilatometry curves. For Ti–6Al–4V, he measures in what he calls equilibrium condition (25 °C/min) a continuous expansion during heating until 950 °C (the maximum temperature in this experiment) with a CTE of $1.1 \times 10^{-5}\,K^{-1}$, during cooling first an increased contraction levelling out to a constant contraction with a CTE of $1.0 \times 10^{-5}\,K^{-1}$. For high heating rates (1000 °C/s!), however, he reports a dilatometry curve similar to the one by Carvalho et al. [38] with $1.1 \times 10^{-5}\,K^{-1}$ up to 900 °C and $0.9 \times 10^{-5}\,K^{-1}$ between 1090 and 1200 °C. He argues that the stalling represents the end of the α to β transformation.

The question arises, to what extent transformations between the α and β phases would influence the length of the material. Basis of the answer is the unit cell volume of the α and β phase. According to XRD measurements (Fig. 5) at room temperature the unit cell volume of the α phase is larger than the one of the β phase. The expansion of the unit cell volume of the α phase with temperature complies with a CTE of $1.1 \times 10^{-5}\,K^{-1}$. The unit cell volume of the β phase expanses in a similar way until 500 °C, and then the expansion accelerates. At the β transus temperature both phases have a similar unit cell volume. This behaviour is in agreement with *in situ* observations of lattice expansion of Ti–6Al–4V using synchrotron radiation by Elmer et al. [35] and with high tem-

perature XRD measurements by Pederson et al. [42]. Elmer et al. report a CTE of $1.0 \times 10^{-5}\,K^{-1}$ at temperatures up to 500 °C and a slightly increased CTE of $1.3 \times 10^{-5}\,K^{-1}$ between 600 and 1000 °C. The important message of the X-ray diffraction results is that the transformation from α to β phase cannot result in expansion as suggested by Tarin et al. [39,40], since the β phase has a smaller unit cell volume. In the contrary, reduced expansion is to be expected. Yet, the change could only be small [42].

Assuming reversibility, during cooling a similar small stalling in the dilatometry curve would be expected due to the β to α transformation. The question is why such a stalling is observed during cooling and not during heating. One reason could be the propensity of Ti to receive oxygen at high temperature. Another reason could be attributed to the non-equilibrium state of the as-fabricated SMD material and to the equilibrium state after the slow TMA experiment (heating and cooling rate of 2 °C/min). In other words the phases could have different compositions before and after TMA. This could have an effect on the amount of β phase, the composition of the α and β phase, residual stresses and others.

It is obvious that oxygen reacts with the Ti alloy in the present TMA experiment. The formation of a α case (Fig. 7(b)), and in the case of the poorer vacuum the one of oxide scales are observed. However, according to the Vickers hardness profile no significant increase in hardness due to alloying of oxygen can be observed in the bulk (Fig. 8). Furthermore, the time at temperature is too small for in-depth diffusion of the oxygen. Hence, the influence of oxygen is restricted to the surface, and can be neglected for TMA, which is not a surface sensitive technique.

It is obvious that the TMA experiment has changed the composition of the phases (Table 2). The α phase is denuded and the β phase is enriched by Vanadium, reaching values in accordance with the equilibrium phase diagram for Ti–6Al–4V [31]. The lattice constants also have changed due to the TMA experiment (Table 1). From these two observations it is deduced that as-fabricated the SMD component is not in the equilibrium state. This non-equilibrium state is not the martensitic α′ phase, since the microstructural analysis suggests a diffusion controlled microstructure, but a non-equilibrium bimodal structure related with a smaller α + β phase field during rapid cooling [34]. This deduction of a non-equilibrium α + β phase field is supported by mechanical spectroscopy experiments (internal friction), where an additional transformation process in as-fabricated SMD material was observed and attributed to the transformation from a non-equilibrium α phase to β phase [29]. If the α phase in equilibrium state has larger lattice constants than the one in the non-equilibrium state, it is imaginable that the transformation into the α phase results in a detectable stalling during cooling, while the transformation from the non-equilibrium does not show. Unfortunately the resolution of HT-XRD was not sufficient and the error too large in order to resolve the small change in length observed by TMA.

5. Conclusions

As-fabricated SMD Ti–6Al–4V components exhibit a constant CTE of $1.17 \times 10^{-5}\,K^{-1}$ during heating up to 1100 °C, where the α to β phase transformation is not reflected. The stalling of the contraction during cooling is attributed to acquiring phase equilibrium at high temperatures with denudation of V in the α phase and enrichment in the β phase. This is taken as indirect evidence that the as-fabricated SMD component contain non-equilibrium composition.

Lattice parameters at room temperature are given as $a = 2.93$ Å and $c = 4.67$ Å for the α phase and $c = 3.20$ Å for the β phase. At room temperature the unit cell volume for the α phase is larger than the one for the β phase. However, with increasing temperature the unit cell volume of the β phase increases strongly in such a way that at 1000 °C both phases have similar unit cell volume.

Acknowledgements

The research is performed within the RAPOLAC STREP project under contract number 030953 of the 6th Framework Programme of the European Commission (www.RAPOLAC.eu), which is gratefully acknowledged. The support of Dr. Rosemary Gault and her team at AMRC, Sheffield, United Kingdom, where the components have been built is highly appreciated.

References

[1] E.W. Collings, The Physical Metallurgy of Titanium Alloys, American Society for Metals, 1984.
[2] M. Long, H.J. Rack, Biomaterials 19 (1998) 1621–1639.
[3] C. Leyens, M. Peters, Titanium and Titanium Alloys, Wiley-VCH, Weinheim, 2003.
[4] R.W. Evans, R.J. Hull, B. Wilshire, J. Mater. Process. Technol. 56 (1996) 492–501.
[5] S.N. Patankar, Y.T. Kwang, T.M. Jen, J. Mater. Process. Technol. 112 (2001) 24–28.
[6] K.M. Taminger, R.A. Hafley, NATO/RTOAVT-139 Specialists' Meeting on Cost Effective Manufacture via Net Shape Processing, NATO, Amsterdam, the Netherlands, 2006, pp. 9–25.
[7] U. Ackelid, M. Svensson, in: Materials Science and Technology (MS&T), Pittsburgh, PA, USA, 2009, pp. 2711–2720.
[8] Arcam, www.arcam.com, 2008.
[9] E. Brandl, C. Leyens, F. Palm, A. Schoberth, P. Onteniente, in: Euro-uRapid, Fraunhofer-Allianz, Berlin, Germany, 2008.
[10] P.A. Kobryn, S.L. Semiatin, J. Mater. 53 (2001) 40–42.
[11] P.A. Kobryn, S.L. Semiatin, J. Mater. Process. Technol. 135 (2003) 330–339.
[12] S.M. Kelly, S.L. Kampe, Met. Mater. Trans. A 35A (2004) 1861–1867.
[13] S.M. Kelly, S.L. Kampe, Met. Mater. Trans. A 35A (2004) 1869–1879.
[14] L. Qian, J. Mei, J. Liang, X. Wu, Mater. Sci. Technol. 21 (2005) 597–605.
[15] S. Nowotny, S. Scharek, E. Beyer, K.-H. Richter, J. Therm. Spray Technol. 16 (2007) 344–348.
[16] G.P. Dinda, L. Song, J. Mazumder, Metall. Mater. Trans. A: Phys. Metall. Mater. Sci. 39A (2008) 2914–2922.
[17] E. Brandl, C. Leyens, C. Dalle-Donne, V. Holzinger, NATO AVTZ-163 Specialists Meeting on Additive Technology for Repair of Military Hardware, NATO/PFP, Bonn, 2009, pp. 1–13.
[18] E. Brandl, C. Leyens, F. Palm, in: Trends in Aerospace Manufacturing (TRAM), Sheffield, UK, 2009.
[19] M. Katou, J. Oh, Y. Miyamoto, K. Matsuura, M. Kudoh, Mater. Des. 28 (2007) 2093–2098.
[20] C. Charles, N. Järvstrat, 11th World Conference on Titanium (Ti-2007), Kyoto, Japan, 2007, pp. 1201–1204.
[21] C. Charles, N. Järvstrat, 8th International Conference on Trends in Welding Research, Pine Mountain, GA, USA, 2008.
[22] D. Clark, M. Bache, M. Whittaker, J. Mater. Process. Technol. 203 (2008) 439–448.
[23] B. Baufeld, A.K. Swarnakar, O. van der Biest, R. Gault, MS&T 2009, Pittsburgh, USA, 2009, pp. 2057–2068.
[24] B. Baufeld, O. van der Biest, Sci. Technol. Adv. Mater. 10 (2009) 10.
[25] B. Baufeld, O. van der Biest, S. Dillien, Met. Mater. Trans. A 41 (2009) 1917–2010.
[26] B. Baufeld, O. van der Biest, R. Gault, Int. J. Mater. Res. 100 (2009) 1536–1542.
[27] B. Baufeld, O. van der Biest, R. Gault, Mater. Des. 31 (2010) S106–S111.
[28] B. Baufeld, O. van der Biest, R. Gault, K. Ridgway, in: TRAM 2009, IOP Conference Series: Materials Science and Engineering, Sheffield, UK, 2010.
[29] A.K. Swarnakar, O. van der Biest, B. Baufeld, J. Mater. Sci., submitted for publication.
[30] S.R. Lampman, in: J.R. Davis, P. Allen (Eds.), ASM Handbook, Vol. 2, Properties and Selection: Nonferrous Alloys and Special-Purpose Materials, ASM International, 1990, pp. 592–633.
[31] R. Boyer, G. Welsch, E.W. Collings, Materials Properties Handbook: Titanium Alloys, The Materials Information Society, 1994.
[32] T. Ahmed, H.J. Rack, Mater. Sci. Eng. A 243 (1998) 206–211.
[33] G. Lütjering, Mater. Sci. Eng. A 243 (1998) 32–45.
[34] R. Banerjee, P.C. Collins, D. Bhattacharyya, S. Banerjee, H.L. Fraser, Acta Mater. 51 (2003) 3277–3292.
[35] J.W. Elmer, T.A. Palmer, S.S. Babu, E.D. Specht, Mater. Sci. Eng. A 391 (2005) 104–113.
[36] I. Weiss, F. Froes, D. Eylon, Met. Mater. Trans. A 15 (1984) 1493–1496.
[37] V.D. Fachinotti, A. Cardona, B. Baufeld, O. Van der Biest, E. Dvorkin, M. Goldschmit, M. Storti, Mecanica Computacional, Vol. XXIX, Asociacion Argentina de Mecanica Computacional, Buenos Aires, Argentina, 2010, pp. 4927–4934.
[38] M.H. Carvalho, H.J. Carvalhinhos, J.F. Thomas Jr., Scr. Metall. 21 (1987) 1417–1422.
[39] P. Tarín, A.L. Fernández, A.G. Simón, J.M. Badía, N.M. Piris, Mater. Sci. Eng. A 438–440 (2006) 364–368.
[40] P. Tarín, I. Alonso, A.G. Simón, J.M. Badía, N.M. Piris, Mater. Sci. Eng. A 481–482 (2008) 559–561.
[41] Y. Robert, Sciences et génie des matériaux, Centre des Matériaux P.M. Fourt, ENSMP, l'Ecole des Mines de Paris, Paris, 2007, pp. 245.
[42] R. Pederson, O. Babushkin, F. Skystedt, R. Warren, Mater. Sci. Technol. 19 (2003) 1533–1538.